Projectile atomic-number effect on ion-induced fragmentation and ionization of fullerenes

O. Hadjar,* R. Hoekstra, R. Morgenstern, and T. Schlathölter†
KVI Atomic Physics, Rijksuniversiteit Groningen, 9747 AA Groningen, The Netherlands
(Received 26 June 2000; published 12 February 2001)

The delocalized π electrons of a C_{60} cluster can be well described as an electron gas. Electronic friction experienced by a multicharged ion colliding with a fullerene might then be modeled in terms of the electronic stopping power. We investigated such collisions for projectile atomic numbers Z ranging from 2 to 18 and charge states $q=2,3$. Direct mass-spectrometric evidence of the clear oscillatory behavior of electronic-stopping-related processes such as multifragmentation and ionization of C_{60} was observed as a function of Z. From the positions of the maxima of the corresponding cross sections, two classes of trajectories can be distinguished: close collisions through the high electron density of the cage inducing multifragmentation, and glancing collisions through the lower electron densities of the fullerene ''atmosphere'' inducing direct ionization.

DOI: 10.1103/PhysRevA.63.033201 PACS number(s): 36.40.Qv, 34.50.Bw, 36.40.Wa

I. INTRODUCTION

The physical properties of clusters and other aggregates of intermediate size can vary over the whole range from those of isolated atoms to those of condensed matter. A lot of effort is directed to understanding the dynamic properties of clusters, especially fullerenes and their ions, interacting with a variety of particles. C_{60} is the most stable cluster in the fullerene family, producible in macroscopic quantities and relatively easy to handle in the laboratory. Photons [1–6], electrons [7–10], as well as neutral [11,12] and charged atomic particles [13], and recently also fast [14–17] and slow [18–24] multiply charged ions have been used to excite C_{60} and observe its response. The dynamic processes involved in these kinds of interaction are very rich and diverse. In contrast to photons and electrons, highly charged ions can produce multiply charged fullerenes with a minimum of energy transfer, leaving the cluster vibrationally and electronically cold. Ninefold-charged C_{60} has been observed in interactions of C_{60} with Bi^{44+} [25] and Xe^{28+} [26], and lately even indications for $C_{60}{}^{10+}$ have been found in collisions with 280-keV Xe^{25+} [27].

C_{60} also offers possibilities of studying processes that are well known from highly charged ion–surface interactions [28], such as resonant electron transfer, hollow-atom formation, and charge-state equilibration. The disadvantage of surfaces and foils is the limited period of time between the projectile's first electron capture and its penetration into the solid. A direct consequence is that only a small fraction ($\sim$10%) of the total relaxation of the system occurs in front of the surface [29]. C_{60} can help to overcome this problem and allow for complete measurements of these processes, since the ions survive after the interaction. The spherical carbon cage of the C_{60} with its delocalized π electrons can be viewed as a microscopic conducting surface.

On the other hand, because of its finite size a net charge is built up due to electron transfer to the projectile, just as in the case of atomic targets. Thus, studies of the interaction of highly charged ions with C_{60} may help to bridge the gap between surfaces and atoms.

From a theoretical point of view, large-impact-parameter processes can be well described by the classical over-the-barrier model. It has been successfully applied to soft collisions between highly charged ions and C_{60} and can explain the behavior of a variety of observables, such as final charge-state distributions and capture cross sections [18,22], as well as projectile deflection angles [20]. Moreover, extensions to this model [30] allow the understanding of the main features in measured projectile kinetic-energy gain spectra [31]: During the projectile-target interaction, the target charge state increases, due to electron-transfer processes, giving rise to a Coulomb repulsion between the projectile and the target, especially on the outgoing trajectory. This repulsion manifests itself in a translational-energy gain, which depends on the number of transferred and stabilized electrons [32]. For projectile charge states of, e.g., ($3.3q$ keV) Ar^{8+}, the energy gain does not exceed 100 eV; however, for higher charge states the energies range up to 150 eV and more [31]. On the other hand the projectiles suffer energy loss mostly due to electronic excitation of the target. Larsson *et al.*, for instance, observed $\sim$800-eV energy loss of 100-keV Ar^{3+} interacting with C_{60} [33]. A typical technique to experimentally study energies involved in the collisions is the analysis of the outgoing projectile's energy. This method by itself does not allow a direct study of how much energy is put into the target system, since projectile energy losses and gains are superimposed.

In our experiment we use the complementary approach of studying the stopping: The energy deposition into the C_{60} is estimated from the relative importance of the subsequent de-excitation processes. In recent studies on He^{q+} ($v=0.1-1$ a.u.) [26,34] and X^{q+} ($Z=2-18$) [35] collisions with C_{60}, we applied an electronic friction model in order to interpret our experimental results. We found that electronic stopping of the fullerene mainly leads to multifragmentation and collisional ionization, whereas at least in the case of the projectiles, evaporation processes are mainly caused by nuclear stopping. For the velocity range under study, multi-

*Electronic address: hadjar@kvi.nl
†Electronic address: tschlat@kvi.nl; URL: kvip56.kvi.nl

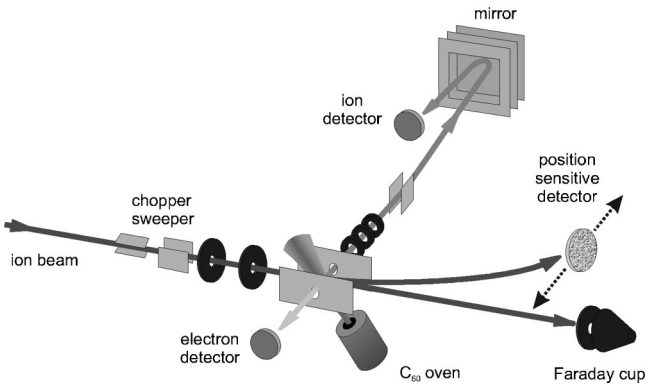

FIG. 1. Schematic of the experimental setup CHEOPS.

fragmentation and direct ionization can therefore be used as fingerprints of electronic stopping and are linked to the amount of energy transferred to the electrons of the target. It has to be noted that Opitz *et al.* [36] observed an opposite behavior of the evaporation yields in a study on proton collisions with C_{60}. This will be discussed in a later section.

The experimental results are compared to theoretical values of the electronic energy loss, based on density-functional theory and a target electron density as obtained from a jellium shell model for C_{60}.

The outline of this paper is as follows. In Sec. II we describe the experimental setup. In Sec. III a brief overview of the electronic stopping is given. The results are presented and discussed in Sec. IV, and Sec. V is the conclusion.

II. EXPERIMENT

In all experiments presented, the two- and threefold-charged ions were extracted from the electron cyclotron resonance ion source (ECRIS) at the atomic physics facility of the KVI. The source is floated at different voltages ($2 \leqslant V_s \leqslant 20$ kV) to obtain an equal velocity ($v = 0.20, 0.25$ a.u.) for all elements. The projectiles used in this study were He, B, C, N, O, F, Ne, Na, S, Cl, and Ar. A sketch of the experimental setup is shown in Fig. 1. The ion beam is collimated by two 1-mm-diameter diaphragms which are 25 cm apart, with the second diaphragm located 8 cm in front of the collision center. The fullerene oven is operated at 700 K. The C_{60} vapor effuses through a nozzle and crosses the projectile ion beam in the collision region. Other target gases can be introduced through a cooled nozzle [37,38]. A static electric field of typically 200 V/cm extracts electrons onto a microsphere plate (MSP) detector, and positive ions through a 4-mm diaphragm into a reflection-type time-of-flight (TOF) mass spectrometer. The detection efficiency of the ion detector (MSP) depends strongly on the impact velocity of the detected ions. The detection efficiency of our detector has been measured to follow the empirical expression

$$D_{\mathrm{eff}}^{\mathrm{MSP}}(m/r) = 1 - \frac{1}{1 + \exp[(115/\sqrt{m/r}) - 5]}, \qquad (1)$$

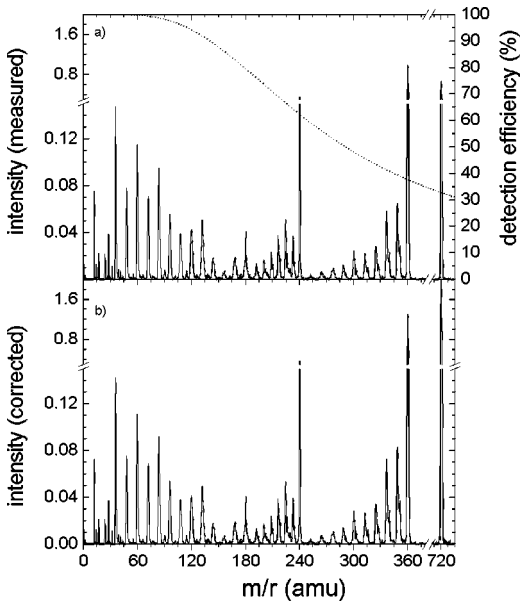

FIG. 2. (a) Raw TOF spectrum converted to an m/r scale measured with a chopped beam of 14-keV N^{2+} projectiles. Superimposed is the detection efficiency (dotted line). (b) Corrected version of the spectrum, differing most at large m/r.

with m and r the mass and the charge state of the detected fragment, respectively. This result is similar to the one obtained previously for a multichannel plate (MCP) detector [21]. TOF measurements can be performed in two modes: (1) with a continuous beam, where the start signal is generated either by a charge-selected outgoing projectile, detected by a movable position-sensitive detector (PSD) situated 70 cm downstream of the collision center, or by an electron originating from the collision; (2) with a pulsed ion beam. The latter technique is mainly used in this work. The projectile beam is periodically deflected to obtain pulses of 20–100 ns length which trigger the TOF measurement. In this way all classes of collision contribute statistically to the spectra. In other words, no discrimination is made between events originating from trajectory classes, differing by charge exchange, scattering angle, and electron emission.

Figure 2 shows a typical raw spectrum obtained in the chopped-beam mode, with the TOF transformed to the mass-over-charge ratio m/r (a). The experimental detection efficiency is plotted as well. Figure 2(b) shows the corrected version of the spectrum. In the following all results presented are detection-efficiency corrected if not stated otherwise. The resolution of the reflection-type mass spectrometer has been improved with respect to our previous studies to $m/\Delta m = 1500$ in the electron-ion coincidence mode. With this resolution, fullerenes containing different numbers of ^{13}C atoms can easily be resolved. The natural abundance of the ^{13}C is 1.11%, implying the yields of $^{12}C_{59}{}^{13}C$, $^{12}C_{58}{}^{13}C_2$, and $^{12}C_{57}{}^{13}C_3$ to be 67%, 22%, and 5% of the $^{12}C_{60}$, respectively.

Figure 3 shows an enlargement of a time-of-flight spectrum, measured in the electron-ion coincidence mode. $^{12}C_{60}{}^{3+}$ and the first three heavier isotopes are clearly visible. The ratio between the three isotope peaks and the $^{12}C_{60}$ peak

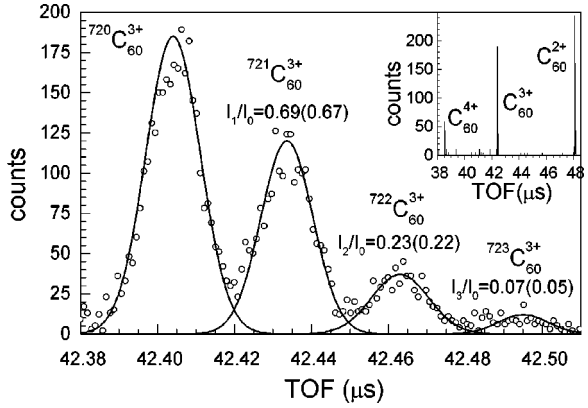

FIG. 3. TOF spectrum measured with a continuous beam of 72-keV O^{6+} projectiles (electron-ion coincidence mode). The inset shows a large part of the spectrum. The 200 cm enlargement around $C_{60}{}^{3+}$ shows the different isotopic constituents with their ratio to the $^{720}C_{60}{}^{3+}$ cluster. The values in parentheses are expected from the binomial formula.

shows good agreement with the expected values. This characteristic distribution can be used to separate parent and fragment peaks in case of identical m/r, e.g., $C_{60}{}^{6+}$ and $C_{10}{}^{+}$. It should be mentioned that a fundamental change observed in electron-ion coincidence measurements with respect to the chopped-beam mode is the absence of the $C_{60}{}^{+}$ peak in the TOF spectra. $C_{60}{}^{+}$ production is mainly due to pure single-electron capture, a process in which no electrons are set free that could serve as a start for the TOF measurements. For the same reason, the whole m/r distribution changes, since products associated with emission of more electrons are overestimated as compared to products where fewer free electrons are produced. These aspects make the method strongly discriminative and quantitative studies over m/r distributions are difficult.

Another essential part of the experiment is the transmission. Our calculations based on the equations of motion applied to particles in the extraction region showed that for an ion exit diaphragm of 4 mm diameter and an extraction of 200 V/cm the transmission is 100%, up to ion kinetic energies of 2 eV. Figure 4(a) shows the transmission as a function of the fragment energy for different field values. Plotted are the transmission functions for forward- and backward-emitted ions. The latter is lower over the whole energy range but converges to the forward transmission at low kinetic energies. Increasing the extraction field brings both transmissions closer together. We define the threshold energy E_{thr} as the maximum energy at which the fragments are transmitted with 100% efficiency:

$$E_{\mathrm{thr}}(\mathrm{eV}) = \frac{D^2}{8L} r E_f . \tag{2}$$

D and L are the diameter of the ion exit diaphragm and the distance between the two extraction plates, respectively, expressed in cm, r is the charge state of the extracted particle,

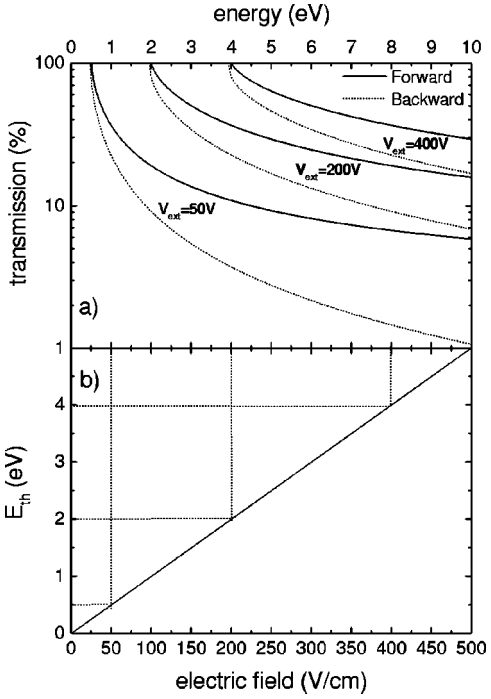

FIG. 4. (a) Transmission function of the detection system for backward- (dotted line) and forward- (solid line) emitted ions. (b) Threshold-energy dependence on the extraction field defined as the highest ion energy detected with 100% transmission.

and E_f is the static electric field in V/cm. Figure 4(b) shows E_{thr} as a function of the applied static electric field for $D = 0.4$ cm, $L = 2$ cm, $r = 1$ a.u.

An increase of the extraction field to 400 V/cm increases the fragmentation yields by less than 7% and 15%, using doubly and triply charged projectiles, respectively, even though the transmission threshold is doubled to 4 eV [see Fig. 4(b)]. This is in agreement with our earlier studies using O^{q+} projectiles [21] and with the results of Opitz *et al.* [32], who also found that only $C_2{}^{+}$ fragments originating from superasymmetric fission exhibit high kinetic energies of up to 5–10 eV. This is an important point, in the sense that if the kinetic-energy release of the fragments changed dramatically the transmission would truncate higher-energy ions, and no direct comparison of the yields obtained with different projectiles was possible.

In the course of this paper, relative cross sections are defined and it is of importance to control reproducibility and stability in time of the spectra. The use of different beam species required total acquisition times of several days over a period of almost three months. To guarantee identical experimental conditions, reference measurements with a 7-kV N^{2+} beam were performed. The exact procedure was the following: after each series of spectra obtained with a specific element, we performed a measurement using N^{2+} projectiles. To verify the reproducibility, the $C_{60}{}^{2+}$, $C_5{}^{+}$, $C_3{}^{+}$, and $C_1{}^{+}$ yields normalized to $C_{60}{}^{+}$ were traced. The recorded differences are within 5%.

III. ELECTRONIC STOPPING

Electronic stopping in ion-solid interactions is a long-established concept. In fact, the use of fast ions as probes of

static and dynamic properties of matter dates almost one century back [39–41]. Bethe showed on the basis of classical considerations that in the high-velocity regime ($v \gg v_F$, with the Fermi velocity v_F), the energy loss per unit length ($S = dE/dX$) of a swift charged particle depends primarily on its velocity v, its nuclear charge Z, the undisturbed electron density n_0, and the mean excitation energy I of electrons making up the stopping medium. More detailed calculations in the framework of linear-response theory followed, introducing the longitudinal dielectric function $\epsilon(k,\omega)$ to describe the medium [42]. For high velocities a classical dielectric function can still be used. At low velocities the full random-phase approximation has been used to describe ϵ [42]. Despite the successive improvements of the description of the medium, the electronic structure of the impinging ions was still poorly described. Ferrell and Ritchie [43] did pioneering calculations and introduced hydrogenic wave functions to calculate the energy loss of He^+ in an electron gas.

The limit of the applicability of linear-response theory is reached at low projectile velocity ($v < v_F$) and low electron-gas density. In this case, bound states start to appear and screen the interactions with the electron gas. This additional effect is well understood within the nonlinear-response theory using density-functional theory [44,45], and the stopping power can be expressed as

$$S = v \frac{3}{k_F r_s^3} \sum_{l=0} (l+1) \sin^2[\delta_l(E_F) - \delta_{l+1}(E_F)]. \qquad (3)$$

Here k_F represents the Fermi wave number and r_s is the electron-density parameter, which is related to the electron density via $r_s = (4\pi n_0/3)^{-1/3}$ (the density parameters for, e.g., solid Al and C are 2.07 and 1.59, respectively [44]). $\delta_l(E)$ are the scattering phase shifts. Due to the complete screening of the nuclear charge Z they obey the Friedel sum rule: $Z = (2/\pi)\Sigma_l (2l+1)\delta_l(E_F)$. Equation (3) introduces a friction coefficient γ via $S = v\gamma(r_s, Z)$. In the velocity range below 1 a.u. the electronic stopping of an ion traversing an electron gas therefore scales linearly with v. For a given density parameter r_s, γ depends solely on the projectile atomic number Z. The electronic structure of an atomic particle embedded in an electron gas can differ from the free-atom case. For $Z = 1-20$, the population of the particle s states is reduced and p or even d states are formed. This leads to a less efficient screening of the core and in the case of a moving particle to an increased electronic stopping. For, e.g., C, N, and O, the p states are unbound or virtual, i.e., they are energetically located within the conduction band. This lowers the screening even more and gives rise to a maximum in electronic stopping. Only the noble gases Ne and Ar keep their atomic properties even when embedded in a (dilute) electron gas. The core is most efficiently screened giving rise to a minimum in the electronic stopping [45]. This phenomenon is known as projectile Z oscillations of the stopping power S. Experimentally, such oscillations have already been observed, e.g., in MeV ion-solid collisions [46,47].

A second aspect is the explicit r_s dependence of γ. With decreasing r_s, i.e., increasing density, minima and maxima shift to higher values. Obviously, for a dilute electron gas in which the perturbation of the projectile by the electron gas is negligible, the minima appear at the Z of the closed-shell rare-gas atoms. With higher electron densities the screening increases and the minima shift to higher nuclear charges since a stronger ionic potential is necessary to compensate for the electronic screening. Figure 5 illustrates these aspects.

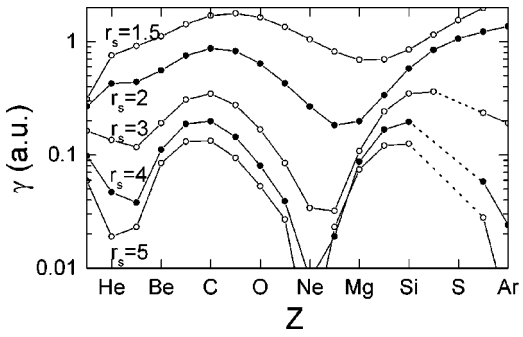

FIG. 5. Theoretical friction coefficient as a function of the atomic number of the moving ion in a surrounding electron gas of different density parameters. Clear oscillations are obvious as well as a systematic increase of the friction with the density.

IV. RESULTS AND DISCUSSION

All results shown in this work are directly extracted from the TOF spectra by peak integration. Figure 2(a) shows a typical m/r spectrum for 14-keV N^{2+} projectiles and a 200-V/cm extraction field. Of the parent peaks ranging from C_{60}^+ to C_{60}^{4+}, the ones with $r \leqslant q$ are mainly due to pure electron capture to the projectile, whereas $C_{60}^{r+}(r > q)$ can only be formed by additional ionization processes. Next to each parent peak, a comblike structure is observed originating from evaporative cooling processes, i.e., a successive loss of C_{2n} units [48]. For He we showed recently that evaporation is mainly caused by vibrational excitation of the C_{60} due to nuclear stopping, in contrast to multifragmentation and direct ionization, which are caused by electronic excitation due to electronic stopping [26,34]. In spite of this, in a recent study Opitz *et al.* [36] found that for the very low nuclear-stopping case of proton projectiles the evaporation shows a velocity scaling similar to the one expected for direct ionization and multifragmentation. In particular, it was found that for protons all deexcitation channels exhibit an electronic-stopping scaling, at least for the velocity range between 0.2 and 3.5 a.u. Maybe also for heavier projectiles a fraction of the evaporation yield is due to electronic stopping. In the following this is of minor importance, since only the multifragmentation and direct ionization will be investigated, which are unambiguously due to electronic stopping.

The $C_{60-2n}^{r+}(r \leqslant q)$ ions are of low relative intensity since the respective parent ions are formed by gentle electron capture. The low-m/r part of the spectrum is dominated by small fragments, ranging from C_1^+ to C_{14}^+. In the following, we use only the sizes smaller than $n = 15$, since, e.g., C_{60}^{4+} and C_{15}^+ overlap in the TOF spectrum. The fit of the corresponding peak by two Gaussians shows a non-negligible contribution of C_{60}^{4+}, which is estimated to be 20% and

50% for doubly and triply charged N projectiles, respectively. However, the contribution of fragments with $n \geqslant 15$ to the total fragmentation yield is estimated to be less than 5% and its neglect is therefore justified. In general, the fragment distribution also shows the typical even-odd oscillations and strong maxima for $n=1$, 3, 5, 7, and 11, as observed for clusters produced directly by laser vaporization of graphite [49].

In order to analyze a set of several spectra obtained using different projectiles, a reliable normalization method is needed. According to the classical over-barrier model the distance at which the projectile captures the first electron from the fullerene depends only on the ionization potential and the polarizability of the fullerene as well as on the charge state of the projectile [50]. In other words, the absolute cross section for the interaction is roughly constant for $Z=2-18$ at equal charge state. We can therefore use the total number of detected particles (Y_{total}) as a reference to define the relative direct ionization and fragmentation cross sections σ_i^q and σ_f^q,

$$\sigma_i^q = \frac{\int {C_{60}}^{i+}}{Y_{\text{total}}}, \quad \sigma_f^q = \frac{\sum_{n=1}^{14} \int {C_n}^{+}}{Y_{\text{total}}}, \tag{4}$$

$$Y_{\text{total}} = \sum_{r=1}^{4} \left[\int {C_{60}}^{r+} + \sum_{n=1} \int {C_{60-2n}}^{r+} \right] + \sum_{n=1}^{14} \int {C_n}^{+}. \tag{5}$$

The choice $i=q+1$ (q being the charge state of the incoming projectile) allows us to separate the first single direct ionization from the gentle-capture processes. Thus, for the series of doubly and triply charged projectiles, the direct ionization cross section is given by the relative yields of ${C_{60}}^{3+}$ and ${C_{60}}^{4+}$, respectively (which are fingerprints of the direct excitation following a close collision of projectile and fullerene). For the fragmentation the same mass range of fragments is used for both projectile charges.

It should be noted that, strictly speaking, the over-barrier model is valid only for large-q projectiles. For $q=2,3$ one could expect influences of the projectile electronic structure on the capture radius. However, if this effect were important, a dramatic change in the cross section would be expected when comparing projectiles as Ne (noble gas) and Na (alkali metal), due to their different electronic structure. Figure 6 reveals that this is not the case; for Ne and Na the relative cross section exhibits no step but follows nicely the predictions of the Z oscillation model, as discussed in the following.

Fragmentation and ionization results for the doubly charged projectile series are shown in Fig. 6. The effect of the electronic stopping power on direct ionization and multifragmentation is clearly seen in the oscillatory behavior of both quantities as a function of Z, as predicted by theory. It is remarkable to see this effect on such small systems with correspondingly short interaction times. The oscillatory behavior of the energy deposition of a projectile traversing an electron gas was predicted theoretically for an infinite homogeneous electron gas such as a solid. The observed oscillations in our interaction system confirm the assumption that multifragmentation and direct ionization are fingerprints of electronic stopping.

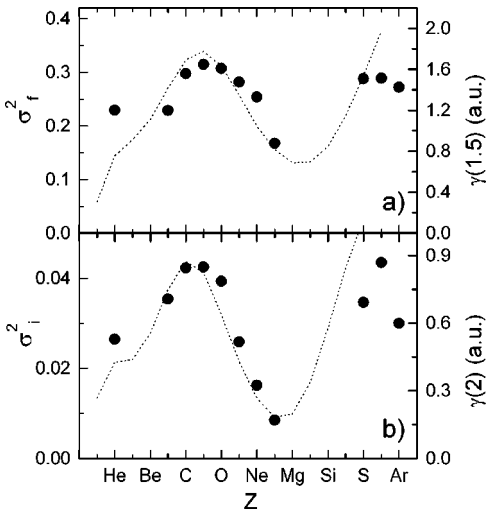

FIG. 6. Relative multifragmentation σ_f^2 (a) and direct ionization σ_i^2 (b) cross sections as a function of the projectile atomic number Z (solid circles). Dotted curves show theoretical friction coefficients to guide the eye. r_s=(a)1.5 and (b) 2.0 a.u.

It could be imagined, however, that fullerene excitation due to enhanced electronic stopping leads not only to stronger fragmentation but also to higher kinetic energies of the produced fragments. This in turn might slightly change the detection efficiencies (see Sec. II). To rule out this possibility we performed electron-ion coincidence measurements and compared the results for the extreme cases of N^{2+} and Ne^{2+}, where high and low fragmentation cross sections, respectively, are observed [see Fig. 6(a)]. The analysis of the fragment peak widths shows no difference between the two spectra. The amount of electronic excitation therefore does not influence the fragment kinetic energies and is reflected only in the fragment yield itself.

Furthermore, from Fig. 6 information can be extracted about the impact-parameter range at which the different processes occur, since they are strongly related to the electron-density profile of the C_{60}. The additional insight into both processes can be obtained from the location of the maxima. It is obvious that σ_f^2 and σ_i^2 peak at different Z values. For instance, the first maximum for σ_f^2 is found at $Z=8$ whereas for σ_i^2 it is found at $Z=7$. Comparing this to the data displayed in Fig. 5 reveals that multifragmentation is due to trajectories through an effective electron-density parameter of $r_s \lesssim 1.5$ a.u., which is in agreement with calculations of Puska and Nieminen [51], who used $r_s=1.2$ a.u. (as a maximum of the electron density around the cage) for a jellium description of the fullerene. Direct ionization takes place in collisions where on the average the probed r_s is larger, i.e., the electron density is lower. Theoretical friction coefficients are plotted as well, to guide the eye, using $r_s=2$ a.u. for direct ionization [Fig. 6(b)] and $r_s=1.5$ a.u. for fragmentation [Fig. 6(a)]. This seems to imply that multifragmentation takes place in collisions where the projectile passes right

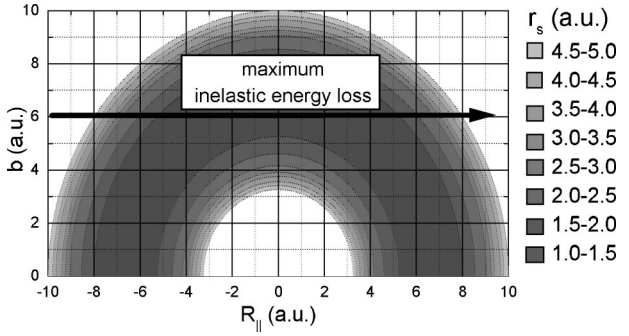

FIG. 7. Contour plot showing the electron density of the C_{60} experienced by the projectile along its path at different impact parameters. The electron density is expressed by the density parameter r_s in gray scale.

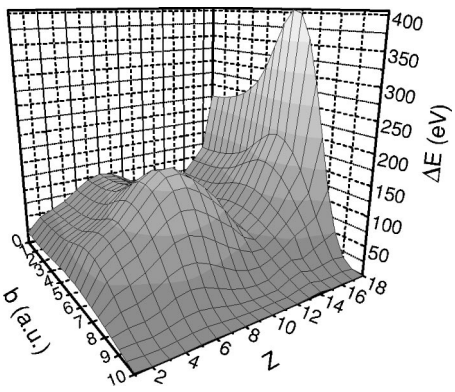

FIG. 8. Total electronic energy loss at 0.2 a.u. projectile velocity as a function of the impact parameter and the projectile atomic number.

through the fullerene cage (high electron density), thereby experiencing bulklike carbon properties, whereas direct ionization is limited to glancing collisions in which the projectile just passes through the electron ''atmosphere'' of the fullerene (low electron density) and the resulting excitation is too small to cause multifragmentation.

To get an idea about absolute values of the electronic stopping, i.e., the energy deposition in the C_{60}, we interpolated the γ values given by Puska and Nieminen [45] using an exponential with two fitting parameters. The friction coefficient can than be described as follows:

$$\gamma(r_s) = A \exp(-Br_s), \tag{6}$$

where A and B are calculated for each Z projectile used and r_s is the calculated C_{60} electron density [51], approximated by the following formula:

$$n_0 = 0.15 \exp[-(R-6.6)^2/2.7]. \tag{7}$$

R is the distance from the fullerene center, which can be expressed in terms of the impact parameter b and the projection of the target-projectile distance onto the incident-projectile direction $R_\parallel$, as $R^2 = b^2 + R_\parallel^2$.

Figure 7 shows a contour plot of the electron-density parameter in these two coordinates. From each impact parameter, a certain average electron density is probed. According to Figs. 6 and 7, direct ionization and fragmentation processes can be assigned to $8 < b < 9$ a.u. and $b \lesssim 8$ a.u., respectively.

The absolute energy loss along a trajectory with given b is calculated in the same way as in a previous work [26], but as a function of the impact parameter and the projectile atomic number, leading to the following expression:

$$\Delta E_{z,b} = v \int_{-\infty}^{+\infty} \gamma_z(r_s(b, R_\parallel)) dR_\parallel . \tag{8}$$

A velocity of 0.2 a.u. is used and the total inelastic energy loss is integrated over $-10 \leqslant R_\parallel \leqslant 10$. Since the electron density of the fullerene decreases rapidly with R, higher absolute values of $R_\parallel$ contribute negligibly to $\Delta E_{z,b}$. Note that for larger impact parameters projectiles with $q = 2,3$ can already capture electrons from the fullerene. As mentioned above, pure electron-capture processes are well described in terms of the classical over-barrier model [24,50]. For our collision systems we find the following capture distances (in atomic units): $R_1^2 = 17.4$ and $R_2^2 = 13.3$ for the doubly charged projectiles and $R_1^3 = 19.4$, $R_2^3 = 15.3$, and $R_3^3 = 12.4$ for the triply charged projectiles.

The results of Eq. (8) are plotted in Fig. 8 as a function of impact parameter b and projectile atomic number Z. Figure 8 shows a clear oscillatory behavior of the total inelastic energy loss as function of Z for all impact parameters. Note that the data for $Z = 16$ are taken as an average between the values for $Z = 15$ and $Z = 17$, since in [45] no convergence was obtained for $Z = 16$. The first maximum exhibits a slight dependence on the impact parameter. A shift toward high-Z values (from $Z = 5$ to 8) is observed as the impact parameter decreases from $b = 10$ to 5.5 a.u., where a maximum of the energy loss is predicted. Smaller impact parameters shift the maximum back to $Z = 7$. This can be understood by considering the average electron density probed by the projectile, which exhibits a maximum at $b = 5.5$ a.u. For smaller impact parameters the energy loss is approximately constant. For $b > 5.5$ a.u. it decreases. Outside the cage ($R_c = 6.7$ a.u.) a strong decrease is observed.

For instance, for 40-keV Ar projectiles, we obtain a maximum energy loss of 400 eV at $b = 5.5$ a.u. This value can be compared to results of Larsson *et al.* [33]. Using the inelastic stopping cross section for 138-keV Ar in graphite (53.4×10^{-15} eV cm^2/atom [52]) and assuming that the projected C atom density in C_{60} is homogeneous over the cage cross section (15×10^{15} cm^{-2}), they derived an average inelastic energy loss of 800 eV for collisions of Ar^{q+} with C_{60}. Because of the linear velocity scaling of the electronic stopping, the 800-eV average electronic energy loss for 138-keV Ar corresponds to an energy loss of 430 eV for 40-keV Ar projectiles, a value that is quantitatively in agreement with the 400 eV predicted by our model. This gives an additional argument for the validity of our model, which can be used as a guideline of the energy losses as a function of the impact parameter. The discrepancy between [33] and our result is probably due to the fact that our model includes a more realistic description of the C_{60} electron-density distribution.

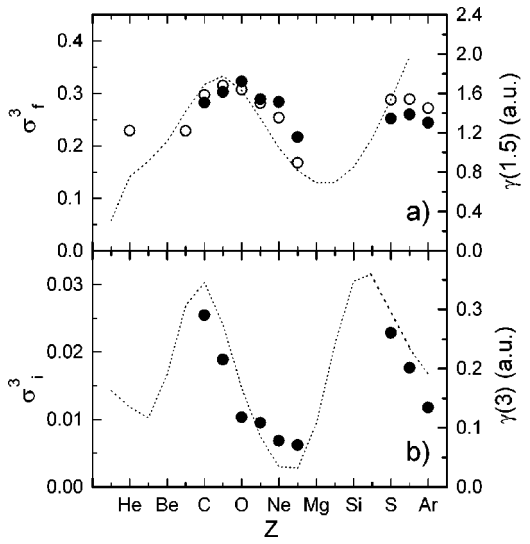

FIG. 9. Same plots as in Fig. 6, obtained with triply charged projectiles. A different density parameter $r_s=3$ a.u. is compared to the direct ionization cross section.

Up to now we have discussed only the electronic stopping of particles with the same charge state $q=2$. It is interesting to investigate how much a variation of q influences the properties of the electronic stopping. For instance, a q-independent stopping would indicate that a quasiadiabatic interaction takes place, in which the projectile has already reached its equilibrium charge state when interacting with the fullerene. A pronounced q dependence, on the other hand, would imply that preequilibrium processes are still active. Figure 9 shows relative cross sections σ_f^3 and σ_i^3 obtained for triply charged projectiles, which can be compared to the data obtained with doubly charged projectiles (Fig. 6.) Qualitatively similar oscillations are observed in both cases. In particular, Fig. 9(a) shows almost no difference in the location of the maximum ($7 \leqslant Z \leqslant 8$) of the fragmentation cross section as compared to doubly charged projectiles. This result is not unexpected since, as mentioned above, multifragmentation occurs for trajectories going right through the cage. The projectiles travel the maximum distance through the fullerene electron gas and experience its maximum density. The equilibrium charge state of the projectile is probably reached.

For direct ionization the situation is different. The excitation energy necessary for a direct ionization of $C_{60}{}^{2+}$ and $C_{60}{}^{3+}$ amounts to 17 and 21.7 eV, respectively [50], i.e., for $q=3$ projectiles about 28% more excitation energy is needed. This is roughly compensated by the 25% stronger electronic stopping due to the increase of the projectile velocity when going from $q=2$ to 3 ($v=0.2$ and 0.25 a.u., respectively). However, comparing Fig. 9(b) and Fig. 6(b), it is seen that the increased projectile charge induces a shift of the first maximum toward lower Z. If we assume that the friction coefficient γ is independent of the projectile q, the results from Fig. 9(b) are best described by $\gamma(r_s=3)$ whereas in the case of $q=2$ projectiles $\gamma(r_s=2)$ gives the best agreement. Figure 5 reveals that, for example, for $Z=7$, $\gamma(r_s=2)$ is about a factor of 3 higher than $\gamma(r_s=3)$. Therefore to be able to put the same amount of electronic stopping into the fullerene, the γ for N^{3+} must be approximately three times higher than for N^{2+} projectiles. Juaristi *et al.* [53] calculated that γ is only 14% higher for N^{3+} than for N^{2+}. An explanation for the observed shift might be that not only do different projectile charge states q have different friction coefficients γ but the positions of the maxima/minima are shifted too. The results of Juaristi *et al.* [53] indicate such an effect. Therefore, calculations of $\gamma(r_s,Z)$ for different projectile charge states q are needed to extract further detailed information on impact parameters from our data. In any case, the q dependence by itself indicates that preequilibrium processes are important.

V. CONCLUSION

Using multiply charged ions, we experimentally studied multifragmentation and direct ionization cross sections of fullerenes in the gas phase. The results were interpreted by means of a statistical electronic-stopping model. The applicability of this model was indicated first by the linearity of these cross sections as a function of the projectile velocity v [34]. Here we presented evidence for an oscillatory dependence of the same cross sections as a function of the atomic number Z (see also [35]), as predicted by theory. This nonlinear effect is a consequence of the nature of the friction parameter γ, which is strongly influenced by the electron-gas-induced screening of the projectile. The oscillatory behavior is therefore strongly dependent on the electron-gas density and the atomic nature of the projectile. The localization of the resonances (maxima) and closed shells (minima) in the cross sections allows us to state that small impact parameters or trajectories going through the C_{60} cage induce multifragmentation. Bigger impact parameters, e.g., glancing collisions, are associated with lower electron densities, giving rise to less friction forces, which are just sufficient to create direct ionization processes. The fragmentation and direct ionization of the fullerene are the result of the energy loss of neutral atoms, which are in different excited states depending on their initial charge state and their nature. The difference of the location of the maxima, when comparing doubly and triply charged projectiles, confirms the dependence of the electronic stopping on the number of projectile L shells, as predicted by Juaristi *et al.* [53]. The higher the number of L shells, the larger the friction coefficient.

ACKNOWLEDGMENT

This project is part of the research program of the Stichting voor Fundamenteel Onderzoek der Materie (FOM) which is supported by the Nederlandse Organisatie voor Wetenschapelijk Onderzoek (NWO).

[1] H. Gaber, R. Hiss, H.-G. Busmann, and I. V. Hertel, Z. Phys. D **24**, 307 (1992).
[2] H. Hohmann, C. Callegari, S. Furrer, D. Grosenick, E. Campbell, and I. V. Hertel, Phys. Rev. Lett. **73**, 1919 (1994).
[3] H. Hohmann, R. Ehlich, S. Furrer, O. Kittelmann, J. Ringling, and E. Campbell, Z. Phys. D **33**, 143 (1995).
[4] S. Hunsche, T. Starczewski, A. L'Huillier, A. Persson, C.-G. Wahlström, H. B. van Linden van den Heuvell, and S. Svanberg, Phys. Rev. Lett. **77**, 1966 (1996).
[5] E. E. B. Campbell, K. Hansen, K. Hoffmann, G. Korn, M. Tchaplyguine, M. Wittmann, and I. V. Hertel, Phys. Rev. Lett. **84**, 2128 (2000).
[6] J. Weaver, J. Martins, T. Komeda, Y. Chen, T. Ohno, G. Kroll, N. Troullier, R. Haufler, and R. Smalley, Phys. Rev. Lett. **66**, 1741 (1991).
[7] B. Dünser, M. Lezius, P. Scheier, H. Deutsch, and T. Märk, Phys. Rev. Lett. **74**, 3364 (1995).
[8] B. Dünser, O. Echt, P. Scheier, and T. Märk, Phys. Rev. Lett. **79**, 3861 (1997).
[9] V. Tarnovsky, P. Kurunczi, S. Matt, T. Märk, H. Deutsch, and K. Becker, J. Phys. B **31**, 3043 (1999).
[10] P. Scheier, D. Hathiramani, W. Arnold, K. Huber, and E. Salzborn, Phys. Rev. Lett. **84**, 55 (2000).
[11] R. Vandenbosch, B. P. Henry, C. Cooper, M. L. Gardel, J. F. Liang, and D. I. Will, Phys. Rev. Lett. **81**, 1821 (1998).
[12] M. Larsen, P. Hvelplund, M. Larsson, and H. Shen, Eur. Phys. J. D **5**, 283 (1999).
[13] A. Reinköster, U. Werner, and H. O. Lutz, Europhys. Lett. **43**, 653 (1998).
[14] T. LeBrun, H. Berry, S. Cheng, R. Dunford, H. Esbensen, D. Gemmell, E. Kanter, and W. Bauer, Phys. Rev. Lett. **72**, 3965 (1994).
[15] H. Tsuchida, A. Itoh, K. Miyabe, Y. Bitoh, and N. Imanishi, J. Phys. B **32**, 5289 (1999).
[16] A. Itoh, H. Tsuchida, T. Majima, and N. Imanishi, Phys. Rev. A **59**, 4428 (1999).
[17] A. Itoh, H. Tsuchida, T. Majima, S. Anada, A. Yogo, and N. Imanishi, Phys. Rev. A **61**, 012702 (2000).
[18] B. Walch, C. Cocke, R. Voelpel, and E. Salzborn, Phys. Rev. Lett. **72**, 1439 (1994).
[19] S. Martin, L. Chen, A. Denis, and S. Desesquelles, Phys. Rev. A **57**, 4518 (1998).
[20] B. Walch, U. Thumm, M. Stöckli, C. Cocke, and S. Klawikowski, Phys. Rev. A **58**, 1261 (1998).
[21] T. Schlathölter, R. Hoekstra, and R. Morgenstern, J. Phys. B **31**, 1321 (1998).
[22] S. Martin, J. Bernard, L. Chen, A. Denis, and S. Desesquelles, Eur. Phys. J. D **4**, 1 (1998).
[23] S. Martin, L. Chen, A. Denis, and S. Desesquelles, Phys. Rev. A **59**, R1734 (1999).
[24] H. Cederquist, A. Fardi, K. Haghighat, A. Langereis, H. Schmidt, S. Schwarz, J. Levin, I. Sellin, H. Lebius, B. Huber, M. Larsson, and P. Hvelplund, Phys. Rev. A **61**, 022712 (2000).
[25] J. Jin, H. Khemliche, M. H. Prior, and Z. Xie, Phys. Rev. A **53**, 615 (1996).
[26] T. Schlathölter, O. Hadjar, J. Manske, R. Hoekstra, and R. Morgenstern, Int. J. Mass. Spectrom. **192**, 245 (1999).
[27] A. Brenac, F. Chandezon, H. Lebius, A. Pesnelle, S. Tomita, and B. Huber, Phys. Scr., **T80**, 195 (1999).
[28] A. Arnau *et al.*, Surf. Sci. Rep. **27**, 117 (1997).
[29] F. W. Meyer, S. H. Overbury, C. C. Havener, P. A. Zeijlmans van Emmichoven, and D. M. Zehner, Phys. Rev. Lett. **67**, 723 (1991).
[30] U. Thumm, A. Barany, H. Cederquist, L. Hägg, and C. Setterlind, Phys. Rev. A **56**, 4799 (1997).
[31] N. Selberg, A. Bárány, C. Biedermann, C. J. Setterlind, H. Cederquist, A. Langereis, M. O. Larsson, A. Wännström, and P. Hvelplund, Phys. Rev. A **53**, 874 (1996).
[32] J. Opitz, H. Lebius, B. Saint, S. Jacquet, B. Huber, and H. Cederquist, Phys. Rev. A **59**, 3562 (1999).
[33] M. Larsson, P. Hvelplund, M. Larsen, H. Shen, H. Cederquist, and M. T. Schmidt, Int. J. Mass. Spectrom. **177**, 51 (1998).
[34] T. Schlathölter, O. Hadjar, R. Hoekstra, and R. Morgenstern, Phys. Rev. Lett. **82**, 73 (1999).
[35] O. Hadjar, P. Földi, R. Hoekstra, R. Morgenstern, and T. Schlathölter, Phys. Rev. Lett. **84**, 4076 (2000).
[36] J. Opitz *et al.*, Phys. Rev. A **62**, 022705 (2000).
[37] R. DuBois, T. Schlathölter, O. Hadjar, R. Hoekstra, R. Morgenstern, C. Doudna, R. Feeler, and R. Olson, Europhys. Lett. **49**, 41 (2000).
[38] H. O. Folkerts, F. W. Bliek, M. C. de Jong, R. Hoekstra, and R. Morgenstern, J. Phys. B **30**, 5833 (1997).
[39] E. Rutherford, Philos. Mag. **21**, 669 (1911).
[40] N. Bohr, Philos. Mag. **25**, 16 (1913).
[41] H. Bethe, Ann. Phys. (Leipzig) **5**, 325 (1930).
[42] P. M. Echenique, R. M. Nieminen, and R. H. Ritchie, Solid State Commun. **37**, 779 (1981).
[43] T. L. Ferrell and R. H. Ritchie, Phys. Rev. B **16**, 115 (1977).
[44] P. M. Echenique, R. M. Nieminen, J. C. Ashley, and R. H. Ritchie, Phys. Rev. A **33**, 897 (1986).
[45] M. J. Puska and R. M. Nieminen, Phys. Rev. B **27**, 6121 (1983).
[46] F. Eisen, Can. J. Phys. **46**, 561 (1968).
[47] P. Hvelplund and B. Fastrup, Phys. Rev. **165**, 408 (1968).
[48] M. Foltin, M. Lezius, P. Scheier, and T. D. Märk, J. Chem. Phys. **98**, 9624 (1993).
[49] J. Gaumet, A. Wakisaka, Y. Shimizu, and Y. Tamori, J. Chem. Soc., Faraday Trans. **89**, 1667 (1993).
[50] A. Bárány and C. J. Setterlind, Nucl. Instrum. Methods Phys. Res. B **98**, 184 (1995).
[51] M. J. Puska and R. M. Nieminen, Phys. Rev. A **47**, 1181 (1993).
[52] B. Fastrup, P. Hvelplund, and C. Sautter, Mat. Fys. Medd. K. Dan. Vidensk. Selsk. **35**, 10 (1966).
[53] J. I. Juaristi, A. Arnau, P. M. Echenique, C. Auth, and H. Winter, Phys. Rev. Lett. **82**, 1048 (1999).